

## Coherence properties of a two-dimensional trapped Bose gas around the superfluid transition

T. Plisson,<sup>1</sup> B. Allard,<sup>1</sup> M. Holzmann,<sup>2,3</sup> G. Salomon,<sup>1</sup> A. Aspect,<sup>1</sup> P. Bouyer,<sup>1,4</sup> and T. Bourdel<sup>1,\*</sup>

<sup>1</sup>Laboratoire Charles Fabry, Institut d'Optique, CNRS, Université Paris-Sud, 2 Avenue Augustin Fresnel, F-91127 Palaiseau CEDEX, France

<sup>2</sup>LPTMC, UMR 7600 of CNRS, Université P. et M. Curie, F-75752 Paris, France

<sup>3</sup>Université Grenoble 1, CNRS, LPMMC, UMR 5493, Boîte Postale 166, F-38042 Grenoble, France

<sup>4</sup>LP2N, Université Bordeaux 1, IOGS, CNRS, 351 Cours de la Libération, F-33405 Talence, France

(Received 14 October 2011; published 19 December 2011)

We measure the momentum distribution of a two-dimensional trapped Bose gas and observe the increase of the range of coherence around the Berezinskii-Kosterlitz-Thouless (BKT) transition. We quantitatively compare our observed profiles to both a Hartree-Fock mean-field theory and quantum Monte Carlo simulations. In the normal phase, the momentum distribution is observed to sharpen well before the phase transition. This behavior is partially captured in a mean-field approach, in contrast to the physics of the BKT transition.

DOI: [10.1103/PhysRevA.84.061606](https://doi.org/10.1103/PhysRevA.84.061606)

PACS number(s): 67.85.Jk, 05.30.Jp, 05.10.Ln

The characteristics of a Bose gas in the degenerate regime are greatly dependent on the dimensionality of the system. In contrast to its three-dimensional (3D) counterpart, a two-dimensional (2D) interacting Bose gas does not present true long-range order at low temperature [1,2]. Instead, it undergoes a superfluid-to-normal-fluid transition described by the Berezinskii-Kosterlitz-Thouless (BKT) theory [3,4]. This superfluid transition has been observed in <sup>4</sup>He films [5], Josephson-coupled superconducting arrays [6], and recently in dilute ultracold atomic gases [7].

In ultracold 2D trapped Bose gases, the appearance of superfluidity was predicted to be preceded by a reduction of density fluctuations [8,9] and by an increase of coherence [10,11]. Experimentally, great efforts have been devoted to the study of the density distribution  $n(\mathbf{r})$  of 2D gases, which gives direct access to the phase-space density and to the density fluctuations. It has permitted the study of the scale invariance [12] and universality in 2D Bose gases [13] as well as their thermodynamics [14]. The study of the first-order correlation function  $g_1$  is possible in real space through interferences between two clouds of atoms [7,15], which revealed its expected algebraic decay in the superfluid regime [7]. The Fourier transform of  $g_1$  is also naturally embedded in the momentum distribution [16,17]. For example, the narrow peak in the density distribution after time of flight is frequently used as an indicator of the slow algebraic decay of the coherence in the superfluid regime [15,18,19].

In this paper, we present a detailed analysis of the experimental momentum distribution of a 2D Bose gas closer to a genuine 2D gas than in previous studies [19]. In addition, we fit our profiles using a Hartree-Fock mean-field (HFMF) model already used in density space [20] but extended here for the momentum distribution, and compare our results to quantum Monte Carlo (QMC) simulations [11,20]. As we increase the phase-space density, we observe a progressive narrowing of the momentum distribution and a change of shape from approximately Gaussian to a peaked distribution, which is not an unambiguous signature of the superfluid phase. In particular, at the superfluid phase transition, the momentum

distribution is already peaked and its width reduced by a factor  $\sim 7$  compared to a Boltzmann thermal gas. Whereas this behavior is partially captured in a mean-field approach where the 2D Bose statistics plays a central role, correlation effects beyond the mean field are clearly visible in the full momentum profile.

Experimentally, the 2D Bose gases are prepared as follows. We prepare a 3D cloud of <sup>87</sup>Rb atoms cooled by all-optical runaway evaporation in a crossed-dipole trap, as described in [21]. During the evaporation process, we turn on a uniform magnetic gradient to select a single hyperfine state ( $|F = 1, m_F = 0\rangle$ ) [22]. We then transfer the cloud to a 2D trap [23]. For that, we adiabatically ramp on a blue-detuned laser at 767 nm in a TEM<sub>01</sub>-like mode, providing an intensity node in the horizontal plane of the atoms (see Fig. 1). It induces a strong confinement in the vertical direction, with an oscillation frequency of  $\omega_z/2\pi = 1.5$  kHz, corresponding to a dimensionless interaction strength  $\tilde{g} = gm/\hbar^2 = \sqrt{8\pi}a_s/a_z = 0.096$ , where  $a_s = 5.3$  nm is the 3D scattering length,  $a_z = \sqrt{\hbar/m\omega_z}$  is the harmonic oscillator length in the vertical direction,  $\hbar$  is the reduced Planck constant, and  $m$  is the atomic mass.

Horizontally, the 2D trap is made of a laser beam at 1565 nm with a waist  $w = 200$   $\mu\text{m}$  and tilted by  $\sim 30^\circ$  with respect to the horizontal plane (see Fig. 1). Its oscillation frequencies are  $\omega_x/2\pi = 8$  Hz,  $\omega_y/2\pi = 15$  Hz. The atom number  $N$  is varied from  $2 \times 10^4$  to  $6 \times 10^4$  by changing the number of atoms initially loaded. The final temperature remains approximately constant at  $T = 64.5 \pm 2.0$  nK. The two-dimensional character of our experiment is given by  $k_B T/\hbar\omega_z = 0.90$  where  $k_B$  is the Boltzmann constant, which results in having  $\sim 70\%$  of the atoms in the ground state of the vertical harmonic oscillator.

We let the atoms thermalize for 500 ms in the final trap before probing the momentum distribution function through time-of-flight (TOF) imaging. In the first milliseconds of expansion, the gas expands predominantly in the vertical direction and the interaction energy is thus quickly released in this direction. As a result, the horizontal momentum distribution (in the  $xy$  plane) remains unchanged during the expansion. After an expansion time of  $t_{\text{TOF}} = 83.5$  ms, much longer than  $1/\omega_x$  and  $1/\omega_y$ , the horizontal density distribution reflects the initial momentum distribution [24]. Finally, two circularly

\*thomas.bourdel@institutoptique.fr

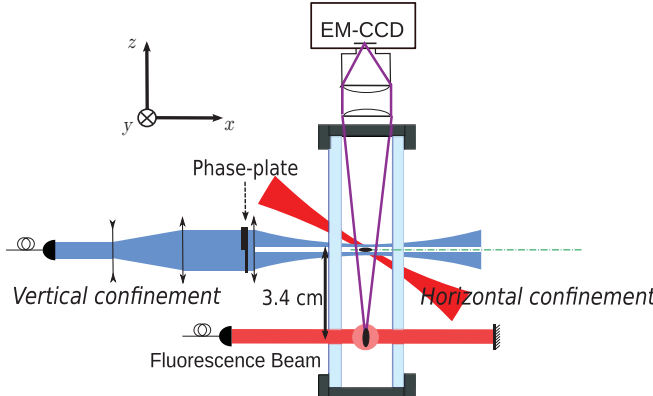


FIG. 1. (Color online) Scheme of the experimental setup. The atom cloud, initially trapped in a harmonic 2D trap with frequencies  $8 \text{ Hz} \times 15 \text{ Hz} \times 1.5 \text{ kHz}$ , is dropped for 83.5 ms before shining a fluorescence beam situated 3.4 cm below the initial position. The fluorescence signal is recorded from above with an electron-multiplying CCD camera.

polarized saturating retroreflected laser beams, resonant with the  $|5S_{1/2}, F = 2\rangle \rightarrow |5P_{3/2}, F' = 3\rangle$  transition and with the  $|5S_{1/2}, F = 1\rangle \rightarrow |5P_{3/2}, F' = 2\rangle$  transition allow the atoms to fluoresce for 100  $\mu\text{s}$ . The fluorescence signal is recorded on an electron-multiplying CCD camera placed along the vertical axis, thus imaging the horizontal profile.

To analyze the experimental data, we perform an azimuthal averaging of the single pictures, as described in [12], in order to extract radial profiles corresponding to the momentum distributions  $n(|\mathbf{k}|)$ , where  $\mathbf{k}$  is the atom wave vector. Experimentally, we weight every point of the profile by its experimental standard deviation (coming from the photon shot noise, the camera dark noise, and the number of averaging points). Such profiles are presented in Fig. 2. For a low atom number [see Fig. 2(e)], the distribution is approximately Gaussian and relatively broad. For a higher atom number [Figs. 2(c) and 2(d)], the curve progressively peaks and deviates from a Gaussian. At high atom number [Figs. 2(a) and 2(b)], a sharp feature develops at very low momentum and grows with increasing atom number. Its width tends to a constant and agrees with our resolution in momentum space (half-width of  $\sim 0.3 \mu\text{m}^{-1}$ ) coming essentially from our imaging resolution and from the initial size of the cloud. Since the peak at low momentum develops on top of a distribution that is not a Gaussian, it is hard to precisely pinpoint when it first appears.

In order to attribute a temperature to each profile, we have to rely on a model. More precisely, we fit the Hartree-Fock mean-field model to the wings of the momentum distribution data. This model has already been used for *in situ* density profiles [11,12,20] but needs to be extended to get the momentum distribution. We proceed as follows. The density distribution in HF MF theory, in the local density approximation, reads

$$n(\mathbf{r}) = \frac{1}{(2\pi)^2} \int_0^\infty \frac{2\pi k dk}{e^{\beta[\hbar^2 k^2/2m + 2gn(\mathbf{r}) - \mu(\mathbf{r})]} - 1}, \quad (1)$$

where  $\beta = 1/k_B T$ , and  $\mu(\mathbf{r}) = \mu_0 - m\omega_x^2 x^2/2 - m\omega_y^2 y^2/2$  is the local chemical potential with  $\mu_0$  the chemical potential at

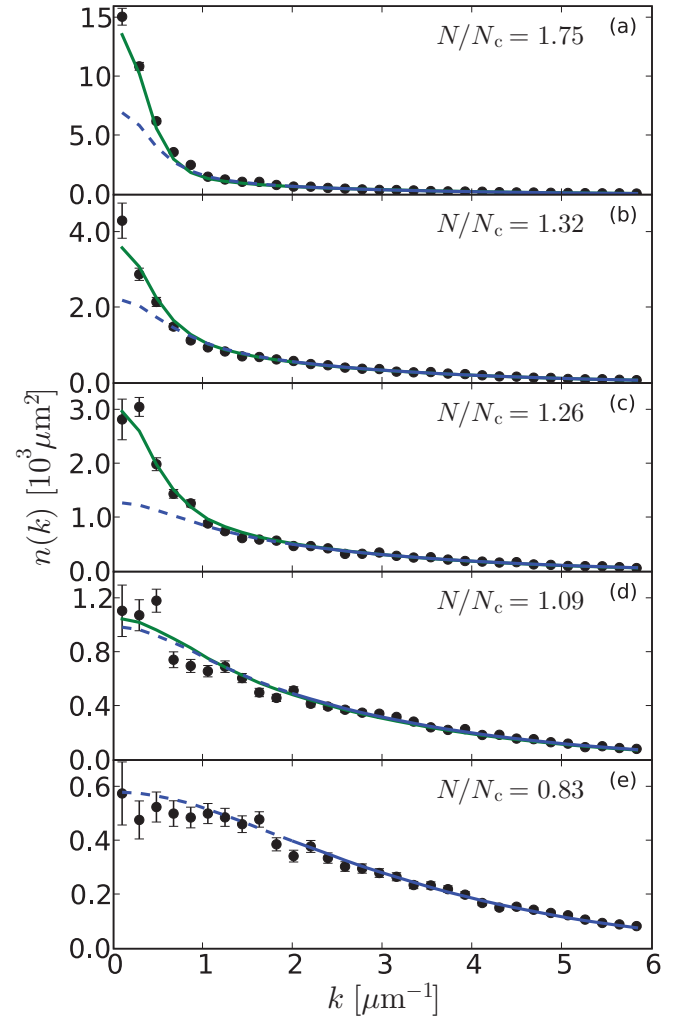


FIG. 2. (Color online) Radial profiles of the momentum distribution for five different atom numbers at constant temperature  $T = 64.5 \pm 2.0 \text{ nK}$ . The atom number  $N$  is given in units of the critical number for the ideal gas Bose-Einstein condensation  $N_c \approx 3 \times 10^4$  and the superfluid phase transition is expected for  $N/N_c \approx 1.26$  (see text). In each plot, we present the experimental data (black dots), the mean-field profiles (blue dashed line) resulting from the fit in the wings (i.e., for  $k > 2 \mu\text{m}^{-1}$ ), and the corresponding quantum Monte Carlo profiles (green continuous line) with the same temperature and the measured atom number.

the trap center. After integration, this leads to the following equation relating  $\mu(\mathbf{r})$  and  $n(\mathbf{r})$  [25]:

$$\beta\mu(\mathbf{r}) = 2\beta gn(\mathbf{r}) + \ln(1 - e^{-\lambda_{dB}^2 n(\mathbf{r})}), \quad (2)$$

where  $\lambda_{dB} = \sqrt{2\pi\hbar^2/mk_B T}$  is the thermal de Broglie wavelength. Writing the momentum distribution

$$n(\mathbf{k}) = \frac{1}{(2\pi)^2} \int \frac{dx dy}{e^{\beta[\hbar^2 k^2/2m + 2gn(\mathbf{r}) - \mu(\mathbf{r})]} - 1} \quad (3)$$

and making the change of variables from  $(x, y)$  to  $\mu$ , we obtain  $n(\mathbf{k})$  after integration. By taking into account the thermally populated vertical levels but neglecting the interaction in these

levels, which is justified since the densities in the excited levels are small, we finally calculate the function

$$n(\mathbf{k}) = \frac{1}{2\pi m\omega^2} \int_{-\infty}^{\mu_0} \frac{d\mu}{e^{\beta[\hbar^2 k^2/2m + 2gn(\mu) - \mu]} - 1} + \sum_{v>0} \frac{-1}{2\pi\beta m\omega^2} \ln(1 - e^{-\beta(\hbar^2 k^2/2m + v\hbar\omega_z - \mu_0)}), \quad (4)$$

where  $n(\mu)$  is determined numerically by solving Eq. (2), and where  $\omega^2 = \omega_x\omega_y$ . For given values of  $\mu_0$  and  $T$ , we can calculate  $n(|\mathbf{k}|)$  and then use this function to fit to the experimental data.

More precisely, we fit the wings of the data where we expect beyond-mean-field effects to play little role and we can extract the temperature and chemical potential. This requires an accurate calibration of the atom detection efficiency, which is a rather difficult task. We have performed QMC simulations based on a numerically exact path-integral algorithm [20,26,27] to calculate the momentum profiles, so that we can adjust the calibration of the atom detector. Within the experimental error bars, it agrees with an independent calibration using the 3D condensation threshold. Moreover, by fitting a mean-field model to the wings of QMC simulations, we find the accurate temperature and thus validate our fitting method.

In Fig. 2, we plot with each profile the fitted mean-field distribution (blue dashed line). We observe that the mean-field fit reproduces well the experimental data at low atom number, while it fails to account for the central part of the profiles when the number of atoms increases. However, the QMC simulations for the fitted temperatures and the experimental atom numbers (green continuous lines in Fig. 2) are in agreement with the experiment in all regimes. For both the calculated mean-field and QMC profiles, we take into account the finite resolution of our imaging system.

In order to quantify the degeneracy of the gas, we calculate  $N/N_c$ , where

$$N_c = \sum_v (\beta\hbar\omega)^{-2} g_2(e^{-v\beta\hbar\omega_z}) \quad (5)$$

is the critical atom number for a noninteracting Bose gas for our trap parameters, and  $g_2(x) = \sum_{n=1}^{\infty} x^n/n^2$ . From classical field calculations [8,9,28], the BKT transition is expected at a central density of the lowest vertical level  $\ln(380.3/\tilde{g})/\lambda_{dB}^2$  with small quantum corrections of order  $\tilde{g}/\lambda_{dB}^2$  [11,20]. Integration of the dominating classical field corrections to the mean field [11] yields  $(N/N_c)_{BKT} \approx 1.26$  as the critical value of the particle number. Close to this value, the experimental profiles are already peaked at low momentum [Fig. 2(c)].

In order to analyze our experimental findings further, we now consider two quantities: the half width at half maximum (HWHM) and the fraction of atoms in the central pixel  $N_0/N$ . The advantage of these two quantities is that they are model independent and quantify the degree of coherence of the gas. The HWHM gives a measure of the inverse of the coherence length, whereas the fraction of atoms in the central pixel is related to the fraction of atoms which are coherent on a length scale larger than  $\sim 5 \mu\text{m}$ . In Fig. 3, we plot these two quantities as functions of  $N/N_c$ . The HWHM is normalized to the HWHM of a Gaussian distribution:

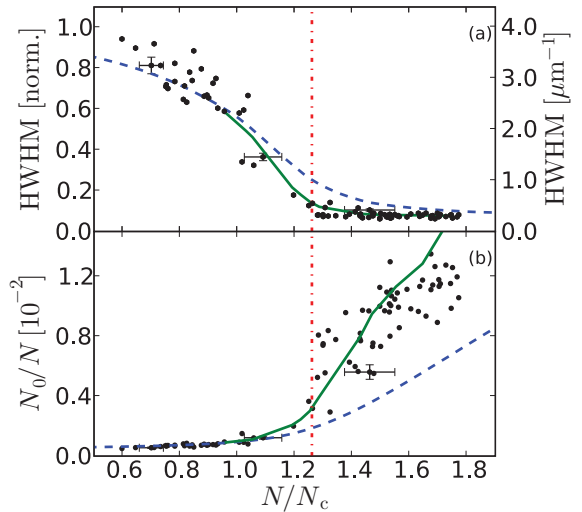


FIG. 3. (Color online) (a) Half width at half maximum of the profiles, normalized to the HWHM of a Gaussian profile for the same temperature, plotted versus the number of atoms normalized to  $N_c$ . (b) Fraction of atoms in the central pixel of the image,  $N_0/N$ . Blue dashed line, mean-field prediction for  $T = 64.5 \text{ nK}$ . Green continuous line, Monte Carlo data for  $T = 64.5 \pm 0.3 \text{ nK}$ . Red vertical dot-dashed line, superfluid transition.

$2\sqrt{\pi \ln(2)}/\lambda_{dB} = 4.0 \mu\text{m}^{-1}$ . Already for  $N/N_c \approx 0.5$ , the normalized width of the momentum distribution starts to decrease from 1. In other words, the distribution is not a Gaussian any more and tends to peak at low momentum. At the superfluid transition point ( $N/N_c \approx 1.26$ ), the HWHM has already decreased by a factor of  $\sim 7$ . After the transition, the HWHM saturates to a value corresponding to the imaging resolution.

The change of shape in the momentum distribution is also reflected in the fraction of atoms in the central pixel [Fig. 3(b)]. This value increases rapidly with the number of atoms. For low atom number, it corresponds to the decrease of the width. For high atom number, while the HWHM saturates, the fraction of atoms in the central pixel keeps growing, reflecting the increasing coherence of the gas with atom number. In our experiment, we finely tune the degeneracy of the cloud and thus resolve the increase of coherence close to the BKT phase transition [19], which does not appear as a sharp feature. This is in contrast to what is predicted for the superfluid fraction [10,25].

In addition to the experimental points, we also plot Monte Carlo simulations and mean-field calculations for our experimental conditions. The Monte Carlo simulations show a good agreement with our experimental findings. The mean-field results coincide with the Monte Carlo simulations at low atom number up to about  $N/N_c \approx 1$ . For high degeneracy parameters  $N/N_c > 1$ , the mean-field model underestimates the height of the coherence peak, showing that beyond-mean-field effects become important. It is remarkable that the mean-field approximation captures the initial increase of the coherence length. This effect is thus not directly linked to the physics of the BKT phase transition for which the theory is inherently beyond mean field. In fact, even in a 2D noninteracting trapped Bose gas, for which calculations are

exact, there is also an increase of the coherence length before the Bose-Einstein phase transition.

The presence of a low-momentum coherence peak cannot be considered as an unambiguous signature of the BKT phase transition. An accurate signature, however, is the slow algebraic decay of the first-order coherence function (as  $1/r^\alpha$  with  $\alpha < 0.25$ ) [7]. This decay can in principle be observed in the momentum distribution, and indeed our QMC calculations show a change of slope (to negative) in the function  $k^{2-\alpha}n(k)$  at low momentum,  $k < \lambda_{\text{dB}}^{-1}$  for  $N \gtrsim 1.3N_c$ , together with the onset of superfluidity. Unfortunately, our experimental resolution is not sufficient for direct observation of this feature.

In conclusion, we have studied the momentum distribution of a trapped interacting 2D Bose gas. In particular, we show that the momentum distribution narrows progressively and well before the BKT phase transition and therefore that a peak in the momentum distribution is not an evidence of the

BKT transition. We also performed a quantitative comparison of the experimental momentum distribution profiles with mean-field and Monte Carlo calculations, strengthening our interpretation. Our detailed characterization of the 2D trapped-Bose-gas momentum distribution will be a useful tool for further studies of the remarkable properties of 2D gases of ultracold atoms.

We thank M. Robert-de-Saint-Vincent for early contributions to the experiment, F. Moron and A. Villing for technical assistance, and J. Dalibard, T. Giamarchi, and W. Krauth for discussions. This research was supported by CNRS, Ministère de l'Enseignement Supérieur et de la Recherche, Direction Générale de l'Armement, Grant No. ANR-08-blanc-0016-01, IXBLUE, RTRA "Triangle de la physique," the EuroQuasar program of the ESF and EU, and iSense. LCFIO is a member of IFRAF.

- 
- [1] N. D. Mermin and H. Wagner, *Phys. Rev. Lett.* **17**, 1133 (1966).
  - [2] P. Hohenberg, *Phys. Rev.* **158**, 383 (1967).
  - [3] V. Berezinskii, Sov. Phys. JETP **34**, 610 (1972).
  - [4] J. M. Kosterlitz and D. J. Thouless, *J. Phys. C* **6**, 1181 (1973); J. M. Kosterlitz, *ibid.* **7**, 1046 (1974).
  - [5] D. J. Bishop and J. D. Reppy, *Phys. Rev. Lett.* **40**, 1727 (1978).
  - [6] D. J. Resnick, J. C. Garland, J. T. Boyd, S. Shoemaker, and R. S. Newrock, *Phys. Rev. Lett.* **47**, 1542 (1981).
  - [7] Z. Hadzibabic, P. Krüger, M. Cheneau, B. Battelier, and J. Dalibard, *Nature (London)* **441**, 1118 (2006).
  - [8] N. Prokof'ev, O. Ruebenacker, and B. Svistunov, *Phys. Rev. Lett.* **87**, 270402 (2001).
  - [9] N. Prokof'ev and B. Svistunov, *Phys. Rev. A* **66**, 043608 (2002).
  - [10] R. N. Bisset, M. J. Davis, T. P. Simula, and P. B. Blakie, *Phys. Rev. A* **79**, 033626 (2009).
  - [11] M. Holzmann, M. Chevallier, and W. Krauth, *Phys. Rev. A* **81**, 043622 (2010).
  - [12] S. P. Rath, T. Yefsah, K. J. Günter, M. Cheneau, R. Desbuquois, M. Holzmann, W. Krauth, and J. Dalibard, *Phys. Rev. A* **82**, 013609 (2010).
  - [13] C.-L. Hung, X. Zhang, N. Gemelke, and C. Chin, *Nature (London)* **470**, 236 (2011).
  - [14] T. Yefsah, R. Desbuquois, L. Chomaz, K. J. Günter, and J. Dalibard, *Phys. Rev. Lett.* **107**, 130401 (2011).
  - [15] P. Cladé, C. Ryu, A. Ramanathan, K. Helmerson, and W. D. Phillips, *Phys. Rev. Lett.* **102**, 170401 (2009).
  - [16] F. Gerbier, J. H. Thywissen, S. Richard, M. Hugbart, P. Bouyer, and A. Aspect, *Phys. Rev. A* **67**, 051602 (2003).
  - [17] S. Richard, F. Gerbier, J. H. Thywissen, M. Hugbart, P. Bouyer, and A. Aspect, *Phys. Rev. Lett.* **91**, 010405 (2003).
  - [18] P. Krüger, Z. Hadzibabic, and J. Dalibard, *Phys. Rev. Lett.* **99**, 040402 (2007).
  - [19] S. Tung, G. Lamporesi, D. Lobser, L. Xia, and E. A. Cornell, *Phys. Rev. Lett.* **105**, 230408 (2010).
  - [20] M. Holzmann and W. Krauth, *Phys. Rev. Lett.* **100**, 190402 (2008).
  - [21] J.-F. Clément, J.-P. Brantut, M. Robert-de-Saint-Vincent, R. A. Nyman, A. Aspect, T. Bourdel, and P. Bouyer, *Phys. Rev. A* **79**, 061406(R) (2009).
  - [22] A. Couvert, M. Jeppesen, T. Kawalec, G. Reinaudi, R. Mathevet, and D. Guéry-Odelin, *Europhys. Lett.* **83**, 50001 (2008).
  - [23] M. Robert-de-Saint-Vincent, J.-P. Brantut, B. Allard, T. Plisson, L. Pezzé, L. Sanchez-Palencia, A. Aspect, T. Bourdel, and P. Bouyer, *Phys. Rev. Lett.* **104**, 220602 (2010).
  - [24] For the detailed analysis of the profiles, we slightly correct  $t_{\text{TOF}}$  to the value  $[(t_{\text{TOF}}^2 + 1/\omega_x^2)(t_{\text{TOF}}^2 + 1/\omega_y^2)]^{1/4} = 85 \text{ ms}$ , to take into account the effect of the initial size. We checked on the mean-field model that this expression corrects the finiteness of  $t_{\text{TOF}}$  at leading order.
  - [25] Z. Hadzibabic and J. Dalibard, *Riv. Nuovo Cimento* **34**, 389 (2011).
  - [26] W. Krauth, *Phys. Rev. Lett.* **77**, 3695 (1996).
  - [27] M. Holzmann, W. Krauth, and M. Naraschewski, *Phys. Rev. A* **59**, 2956 (1999).
  - [28] M. Holzmann, G. Baym, J.-P. Blaizot, and F. Laloë, *Proc. Natl. Acad. Sci. USA* **104**, 1476 (2007).